Effect of alloy matrix on the mechanical properties and deformation mechanisms of aluminum foams

Ming-fang Zhu¹, *Ning-zhen Wang^{1,2}, Wen-sheng Fu³, Ru-yuan Yang¹, Peng Zhang³, *Liang Tang^{1,2} and *Xiang Chen³

- 1. School of Technology, Beijing Forestry University, Beijing 100083, China
- 2. State Key Laboratory of Efficient Production of Forest Resources, Beijing 100083, China
- 3. School of Materials Science and Engineering, Tsinghua University, Beijing 100084, China

*Corresponding address: e-mail: ningzhenwang@bjfu.edu.cn, happyliang@bjfu.edu.cn, xchen@tsinghua.edu.cn

Abstract: This study systematically evaluates the role of AlSiMg and AlCa alloy matrix composition in determining the mechanical properties, energy absorption, and deformation mechanisms of closed-cell aluminum foams. Quasi-static compression tests coupled with digital image correlation (DIC) were employed to analyze the full-field strain distribution and deformation behavior. Compared to AlCa foams, the initial peak stress and plateau stress of AlSiMg foams at the relative density ρ r=0.26 are 1.9 and 1.3 times higher, respectively. These enhancements were attributed to solid-solution strengthening and hard-phase reinforcement (Mg₂Si, Si, and MgAl₂O₄), which also induced brittle fractures during compression and led to stress fluctuations in the stress-strain curves. AlCa foams exhibited smooth stress-strain curve, and their energy absorption capacity were demonstrated better energy absorption at lower densities (ρ r=0.22–0.23) due to their better plasticity of the matrix. DIC results also revealed distinct deformation modes of the two kinds of aluminum foams. AlSiMg foam followed a "Hard-phase support—Brittle fracture" mechanism, with crack propagation along hard-phase interfaces, while AlCa foam exhibited "Plastic coordination—Progressive buckling", enabled by uniform pore distribution and ductile matrix. Therefore, the alloy matrix critically governs the foam performance, with hard phases enhancing strength but weakening ductility in AlSiMg foams. This work provides fundamental insights for designing matrix alloys to tailor foam properties for energy-absorbing applications, highlighting the trade-offs between strength and toughness in aluminum foams.

Keywords: Aluminum foams; Casting-foaming method; Alloy matrix; Mechanical properties

1 Introduction

Closed-cell aluminum foams have attracted considerable attentions in the automotive, transportation, aerospace and architectural fields due to their low density, energy absorption, sound insulation, electromagnetic shielding, and thermal insulation capabilities [1,2]. Aluminum foams prepared by traditional methods can only be used in form of specific shapes by mechanical processing, which is difficult to obtain complex shapes [3-5]. Novel casting foaming methods offer a promising approach for fabricating aluminum foam components with controlled porosity and superior mechanical properties [6,7]. Given the good fluidity and low cost, AlSi alloy was selected as the base material for casting foaming. The

conventional thickening agent Ca exhibits limited solubility in Al-Si alloys and tends to react with Si to form CaSi₂Al₂ intermetallics. This reaction consumes Ca and consequently reduces its foam-stabilizing effectiveness, making Ca unsuitable for Al-Si-based foams. Therefore, Mg was used as an alternative [8,9]. The mechanical properties of aluminum foams primarily depend on the pore structure (including porosity, cell size, and cell morphology) and the matrix properties, with the latter playing a critical role [10,11]. Therefore clarifying the interaction between alloy selection and manufacturing techniques is essential for expanding their functional applications.

The composition, structure, and spatial distribution of the matrix alloy are critical factors that influence the mechanical performance and deformation behavior of aluminum foams [12,13]. Ashby and Gibson [14] observed that the elastic modulus, yield strength, and other properties of foam materials are proportional to those factors of the matrix material. Cheng et al. [15] found that, at the same relative density, AlZn28 foams exhibit superior mechanical properties and energy absorption capacity compared to AlMg10 foams. Cheng et al. [16] reported that AlSiCu foams exhibit an increase in flow stress after yielding, resulting in a sharp rise in energy absorption. Huang et al. [17] demonstrated that adding 0.2% Sc and applying T6 heat treatment improved the strength of Al-Sc foams by 22%. Xia et al. [18] observed that AlMn foams with 1.0% Mn content had a yield strength approximately 4.2 times higher than that of pure aluminum foams; when the Mn content was increased to 4.0%, the energy absorption capacity of the AlMn foam was about 5.6 times that of the pure aluminum foam. Zhao et al. [19] conducted a systematic study on the effect of Er and found that when the Er content ranged from 0.10 to 0.50 wt.%, AlEr foams achieved an optimal balance between compressive strength and energy absorption, exhibiting a trend of initial increase followed by a decrease.

Previous studies have demonstrated that Mg addition can effectively enhance the matrix properties of aluminum foams. Fusheng et al. [20] found that adding Mg to the matrix improved foam strength but decreased ductility, leading to brittle fracture and cell wall collapse. Lin et al. [21] reported that increasing the Mg content from 0 wt% to 6 wt% enhanced the peak compressive strength of AlMg foams by 76.3%. Lohani et al. [22] used AA6061 aluminum alloy (Al-Si-Mg system) as the matrix and added Al₂O₃ as a stabilizing agent to refine the pore structure. Their results showed that AlSiMg foams with 10 wt% Al₂O₃ exhibited cell sizes ranging from 1.2 to 5.8 mm, a plateau stress of 30.68 MPa, a broader plateau strain range, and a smoother energy absorption process. Currently, most melt foaming methods use pure aluminum with Ca as a thickening agent, resulting in AlCa-based foams that exhibit good foaming behavior and mechanical properties [23,24]. However, the casting foaming method employs an AlSiMg alloy matrix, and research on the

mechanical properties of foams prepared from this alloy remains limited.

This study investigates the compressive properties, energy absorption characteristics, and microstructure of AlSiMg foam prepared by the casting foaming method, and compares it with the traditional AlCa foams fabricated via the melt foaming method. Digital image correlation (DIC) technology was employed during quasi-static compression tests to capture full-field strain distributions and reveal the deformation mechanisms of both foams. Scanning electron microscopy (SEM) was used to examine their microstructures and elucidate the role of matrix strengthening phases. By correlating macroscopic mechanical responses with microstructural features, this study offers new insights into matrix alloy design and contributes to the development of aluminum foams for applications in impact resistance and energy absorption.

2 Materials and methods

2.1 Specimen preparation

AlCa foams and AlSiMg foams were used in this study. The raw materials for preparing AlCa foam were pure Al (purity > 99.5%), dustry pure (99.7%) AlMg50, pure Ca (granule size $2 \sim 4$ mm, purity > 98%), and TiH₂ powders. AlCa foams were prepared using the melt foaming method. The process involved melting pure Al, adding Ca to increase the melt viscosity, and subsequently introducing an AlMg-35TiH₂ composite foaming agent synthesized from AlMg50. The AlCa foams were obtained after a holding period followed by cooling [25].

The raw materials for preparing AlSiMg foam were pure Al (purity > 99.7%), AlMg50 master alloy and AlSi30 master alloy ingots, and TiH₂ powders. AlSiMg foams were prepared using the casting foaming methods. The foamable precursor alloy was prepared by dispersing TiH₂ particles into a thickened Al-Si-Mg eutectic melt. The mixture was cast into a preheated mold, foamed to fill the cavity, and finally solidified to produce AlSiMg foam [6-8].

2.2 Characterization methods

The specimen size was chosen to be a cube with a side

length of 30 mm to ensure that more than seven cells were present in the loading direction, thereby avoiding size effects. A field emission scanning electron microscope (SEM, Zeiss Gemini SEM 500) was used to characterize and analyze the morphology and phase composition of aluminum foams prepared with two different alloy matrices.

2.3 Quasi-static compressive test

Quasi-static compressive testing was conducted on a C45-100 computer-controlled electronic universal testing machine (MTS Industrial Systems Co., Ltd.). The experimental setup is shown in Fig. 1a. The compressive rate was set at 2 mm/min with a compressive strain rate of 1.1×10^{-3} s⁻¹, and the load-displacement curves were recorded automatically. A 3D digital image correlation (DIC) system, capable of capturing the deformation process *in situ*, was used to measure the deformation behavior of the aluminum foams. White and black speckles were randomly applied to the specimen surface to create a high-contrast pattern, thereby significantly enhancing the clarity of the deformation process visualization. The collection

frequency by camera was set to 5 Hz. The aluminum foam specimen is shown in Fig. 1b.

The plateau stress σ_P of aluminum foams was used to characterize their mechanical properties and was calculated by Eq. (1). The energy absorption per unit volume W and energy absorption efficiency η were employed to evaluate the energy absorption capacity of aluminum foams, and can be calculated using Eqs. (2) and (3), respectively.

$$\sigma_{\rm P} = \frac{\int_{\varepsilon_0}^{\varepsilon_{\rm D}} \sigma(\varepsilon) \mathrm{d}\varepsilon}{\varepsilon_{\rm D} - \varepsilon_0} \tag{1}$$

Where ε_0 is the strain corresponding to the first peak stress in the curve. ε_D is the densification strain, with its detailed calculation process described in [26].

$$W = \int_0^{\varepsilon_{\rm D}} \sigma(\varepsilon) d\varepsilon \tag{2}$$

$$\eta = \frac{\int_0^{\varepsilon_{\rm D}} \sigma(\varepsilon) d\varepsilon}{\sigma(\varepsilon)}$$
 (3)

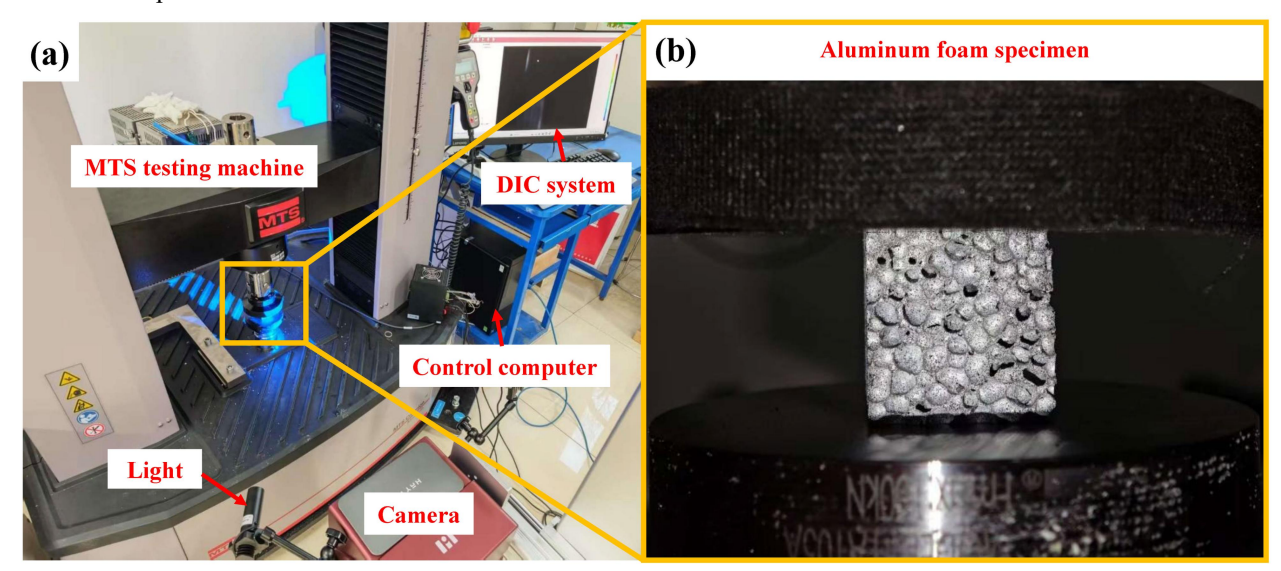


Fig. 1: Schematic of the experimental process: (a) Quasi-static experimental setup, and (b) an aluminum foam specimen.

3 Results and discussion

3.1 Compressive stress-strain curve

Quasi-static compression tests are commonly used to evaluate the mechanical properties and energy absorption capacity of aluminum foams. Owing to their cellular structure, the compression deformation process typically consists of three stages: the linear elastic stage, the plateau stage, and the densification stage [27]. Fig. 2 presents the stress–strain curves of AlCa and AlSiMg aluminum foams

As shown in Fig. 2a, the initial peak stress (IPS)

increases with relative density, ranging from approximately 8.6 to 14.8 MPa with the densities from 0.22 to 0.29. The curves display a distinct yield point followed by a plateau region. With increasing relative density, the plateau stress increases, but the length of the plateau region gradually decreases, suggesting that higher-density foams enter the densification stage earlier.

In contrast, the AlSiMg foams (Fig. 2b) exhibited a more complex stress-strain response. At a relative density of 0.25, the IPS reached 28.7 MPa, nearly twice that of the AlCa foam (relative density of 0.29, 14.8 MPa). Fluctuations observed in the plateau region remained below the IPS value,

suggesting the occurrence of brittle failure during compression.

The results indicate that the plateau stress of both AlCa and AlSiMg foams increases with increasing relative density. However, the stress-strain curve of AlSiMg foams exhibits pronounced fluctuations, which are attributed to the matrix compositions. Therefore, this study further analyzes and discusses the influence of the alloy matrix on the mechanical and energy absorption properties of from the perspectives of aluminum foams microstructure and macroscopic deformation behavior.

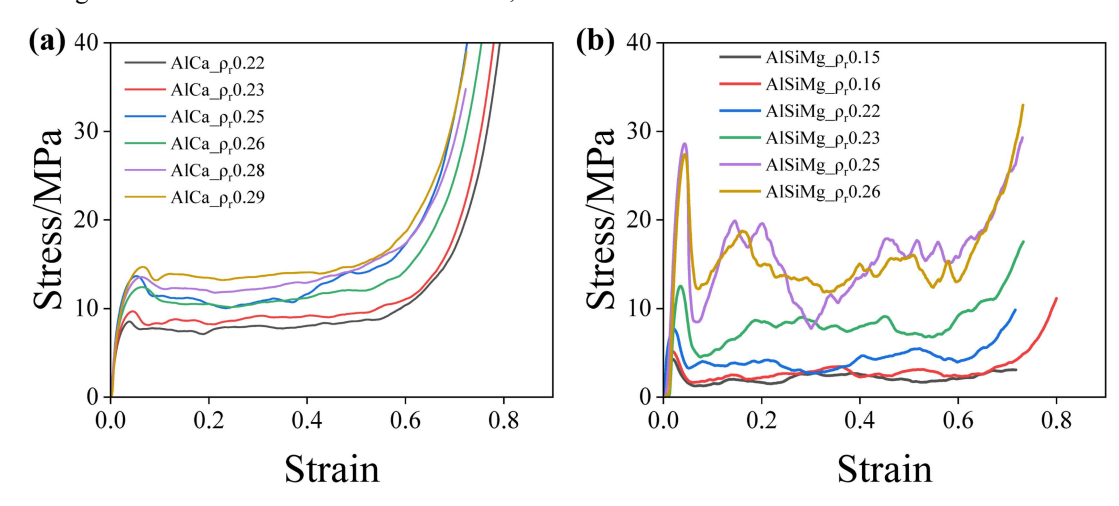


Fig. 2: Quasi-static compression stress-strain curves of (a) AlCa foams and (b) AlSiMg foams. (pr is the relative density)

3.2 Effect of matrix materials on mechanical properties of aluminum foams

As shown in Fig. 3, the stress–strain curves of AlCa and AlSiMg foams with the same relative densities (0.22, 0.23, 0.25, and 0.26) are presented. Fig. 4 displays the corresponding plateau stresses and IPS. It can be observed from Figs. 3 and 4 that at lower relative densities (ρ_r = 0.22 and 0.23), the plateau stress σ_P of AlCa foams is higher than that of AlSiMg foams. However, at higher relative

densities ($\rho_r = 0.25$ and 0.26), the plateau stress σ_P of AlSiMg foam exceed that of AlCa foam. Specifically, at $\rho_r = 0.26$, the σ_P of AlSiMg foam is approximately 1.3 times that of AlCa foam. Except at $\rho_r = 0.22$, the IPS of AlSiMg foams consistently exceeds that of AlCa foams. Furthermore, the difference in IPS between the two materials increases with increasing relative density, reaching more than twice at $\rho_r = 0.26$.

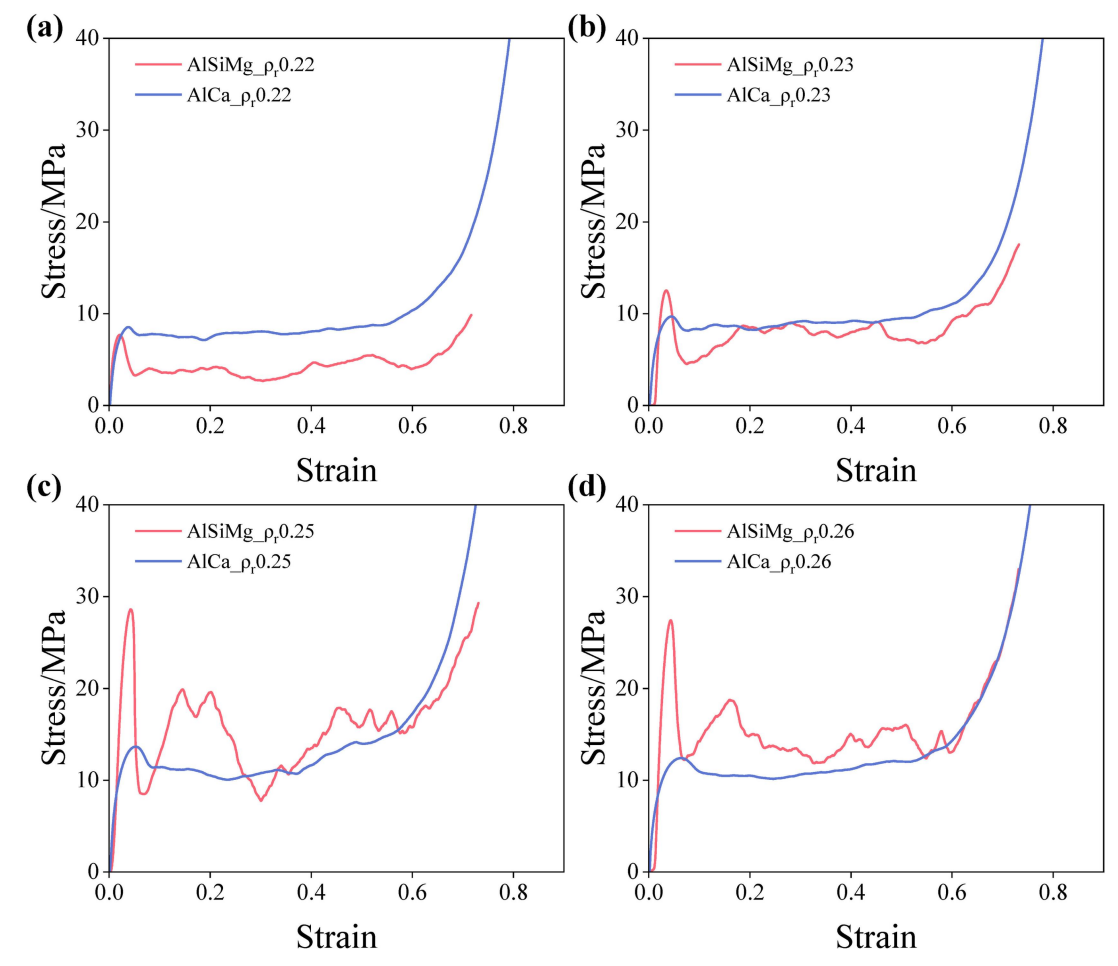


Fig. 3: Comparison of stress–strain curves between AlCa and AlSiMg foams under quasi-static compression, with (a)–(d) corresponding to pr= 0.22, 0.23, 0.25, and 0.26, respectively.

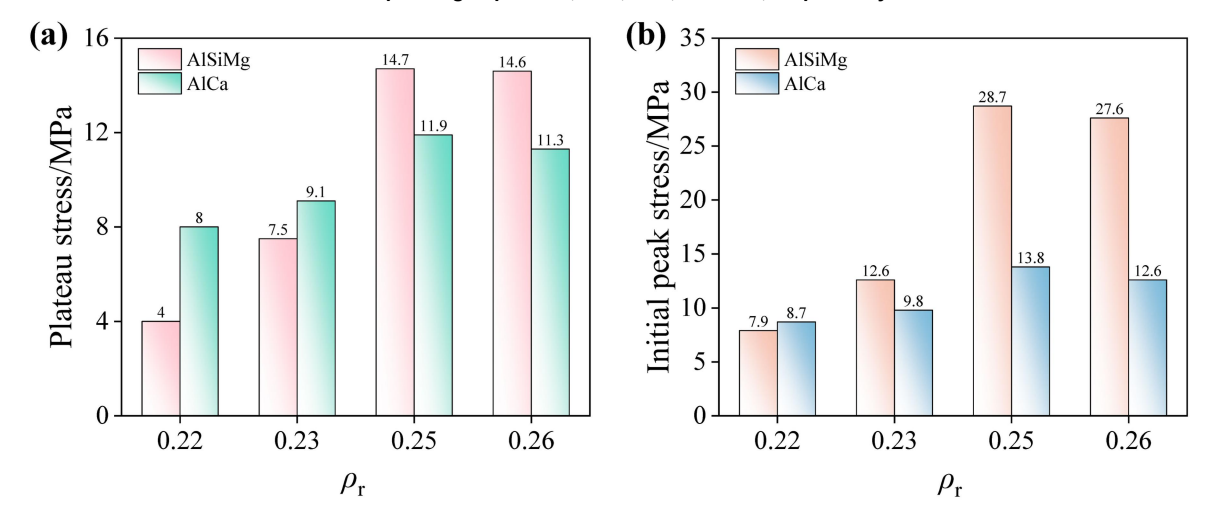


Fig. 4: Comparison of plateau stress (a) and initial peak stress (b) between AlCa and AlSiMg foams.

To investigate the causes of brittle fracture in the cell walls and the differences in compressive performance between AlCa and AlSiMg foams, the microstructures of the specimens were examined and analyzed. Their SEM images are presented in Fig. 5.

The size and distribution of second-phase particles within the alloy matrix are critical factors influencing the mechanical properties of aluminum foams [28]. As shown in Fig. 5a, the microstructure of AlCa foam primarily consists of the primary α -Al phase, the Al₄Ca phase, and dark Bi-film oxide

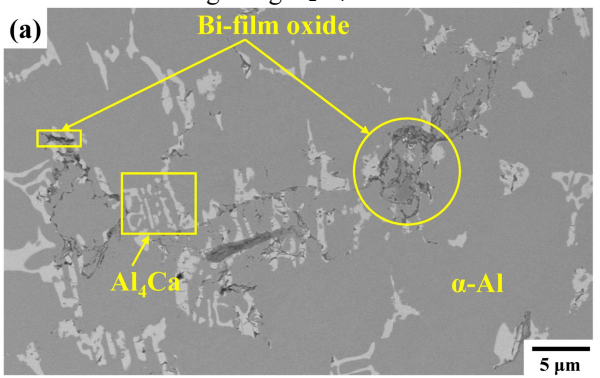
phases, with the shade and morphology of the Bi-film oxide related to the oxygen content. The eutectic Al₄Ca phase forms a continuous fibrous structure that is uniformly distributed within the aluminum matrix. Its effects on the mechanical properties of the aluminum foam are reflected in the following two aspects. Firstly, the strong metallic bonding between Al₄Ca and α-Al enhances interfacial adhesion, resulting in a more uniform stress distribution that delays local plastic deformation or fracture, thereby improving the foam's strength and ductility. Secondly, the uniform distribution of the eutectic Al₄Ca phase effectively hinders crack propagation, thus enhancing the impact resistance of the aluminum foam.

As shown in Fig. 5b, the AlSiMg foam primarily consists of four phases: the primary α-Al phase, irregular blocky eutectic Mg₂Si phase, light gray eutectic Si phase, and bright white granular MgAl₂O₄ phase. The MgAl₂O₄ spinel particles are mainly distributed within the Al-Si-Mg₂ Si eutectic regions and are absent within the primary α-Al grains. The superior mechanical performance of the AlSiMg foam originates from the effect of the presence of hard second phases (eutectic Mg₂Si and eutectic Si phases) in the as-cast matrix. The hard Si/Mg₂Si skeleton effectively enhances the compressive strength of the cell walls ^[29,30]; however, the brittleness of the eutectic silicon limits their ductilitAlthough MgAl₂O₄ nanowhiskers can

enhance mechanical properties, the MgAl₂O₄ in Fig. 5b exists as micron-sized spinel particles, primarily concentrated in the Al-Si-Mg₂Si eutectic region. As a brittle oxide, MgAl₂O₄ exhibits poor interfacial bonding with the surrounding Al-Si-Mg₂Si phases. During compression, cracks tend to propagate along the MgAl₂O₄ particles, leading to interfacial brittle fracture. The MgAl₂O₄-rich regions become centers of local collapse, which is manifested macroscopically as localized pore collapse and significant fluctuations in the stress-strain curves. Additionally, AlSiMg foam contains more defects, such as holes and cracks, which can exacerbate the fluctuations in the stress-strain curve.

At lower relative densities ($\rho_r = 0.22$ –0.23), the cell walls per unit volume are thinner, and the limited number of hard phases in the AlSiMg foam can act as defect sites that initiate cracks, leading to brittle fracture of the cell walls and making the foam more prone to collapse under compression.

At higher relative densities ($\rho_r = 0.25$ –0.26), the cell walls per unit volume become thicker, and the content of hard Si/Mg₂Si phases in the matrix is high enough to strengthen the AlSiMg foam. Although AlCa foam still exhibits superior ductility at this stage, its overall strength is insufficient. As a result, the AlSiMg foam shows better mechanical performance.



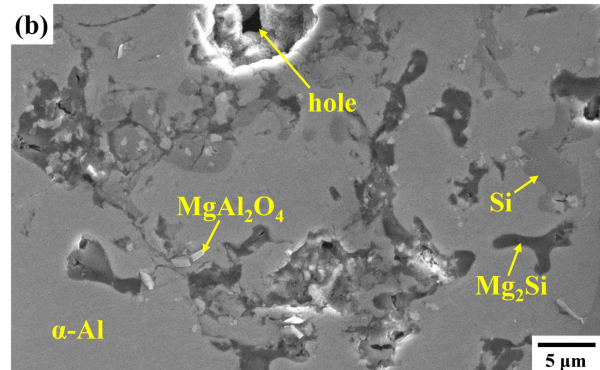


Fig. 5: SEM images of aluminum foams with different matrices: (a) AlCa foam, (b) AlSiMg

3.3 Effect of matrix materials on energy absorption properties

The energy absorption properties of AlCa foam and

AlSiMg foams with different densities are shown in Fig. 6a. At lower relative densities (ρ_r =0.22, 0.23), AlCa foams exhibit superior energy absorption

performance compared to AlSiMg foams with the same relative density. This is primarily because, at lower relative densities, the thin cell walls deform mainly through bending, buckling, and plastic hinge formation. In this regime, the high ductility of the matrix permits extensive plastic deformation of the cell walls without fracture, thereby enhancing energy absorption through plastic work. Additionally, the softer Al₄Ca phase (~300 HV) matches better with the α-Al matrix compared to the hard and brittle Si phase (~1000 HV) in AlSiMg foams, leading to stronger cooperative deformation and more gradual wall buckling, thus extending the plateau region. In contrast, at lower relative densities, the hard phases (Si/Mg2Si) in AlSiMg foam are sparsely distributed and fail to form an effective supporting network, leading to premature local brittle fracture and lower energy absorption capacity.

At higher relative densities (ρ_r =0.25, 0.26), AlSiMg foams exhibit superior energy absorption performance due to the cooperative strengthening of the hard phases. As the relative density increases, the deformation of the foam shifts from plastic hinge formation in the cell walls to layer-by-layer compaction. The high strength of AlSiMg enables sustained compression at higher stress levels, thereby enhancing energy absorption efficiency. Furthermore, with increased relative density, the cell wall thickness grows. Although the AlCa foam still undergoes plastic deformation, its insufficient strength leads to a lower stress plateau during densification (as manifested by the gentle slope in the compression curve), resulting in reduced energy absorption. However, as the wall thickness increases, the hard Si/Mg₂Si phases and MgAl₂O₄ oxide particles accumulate, leading to brittle fracture of the foam walls. This is reflected in fluctuations in the energy absorption efficiency curve, as shown in Fig. 6b, where the maximum energy absorption efficiency of the AlSiMg foam is more than twice that of the AlCa foam at the same relate density of 0.26.

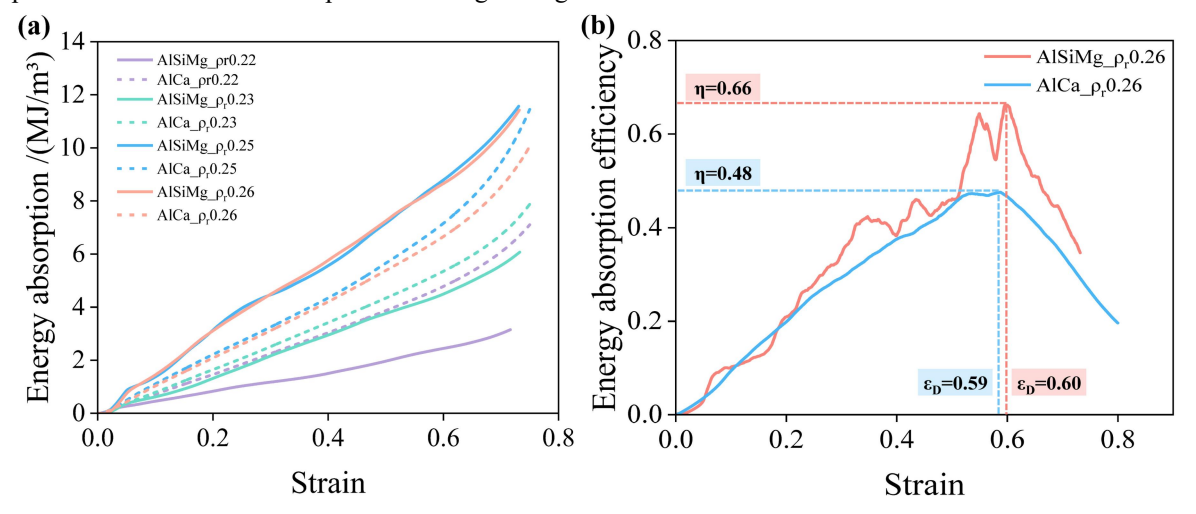


Fig. 6: (a) Energy absorption per unit volume plots of AlCa and AlSiMg foams. (b) Energy absorption efficiency of AlCa foam and AlSiMg foam at a relative density $\,
ho \, r \, = 0.26$.

3.4 Deformation mechanisms of aluminum foams with different matrixes

To investigate the deformation mechanisms of AlCa and AlSiMg foams, cross-sectional images of both foams with a relative density of 0.26 were binarized prior to quasi-static compression testing. The resulting pore structures are depicted in Fig. 7a and 7b, which clearly reveal that the pore walls of the

AlSiMg foam exhibit unevenness, with localized thickening (as indicated by arrows), attributed to the clustering of hard Si/Mg₂Si phases (bright regions in the SEM images). In comparison, the difference in cell wall thickness of normal cell walls and Plateau borders in the AlCa foam is relatively small. Furthermore, the cells within AlSiMg foam are characterized by a larger diameter

and a reduced number, yet they display a better cell roundness when contrasted with those in the AlCa foam.

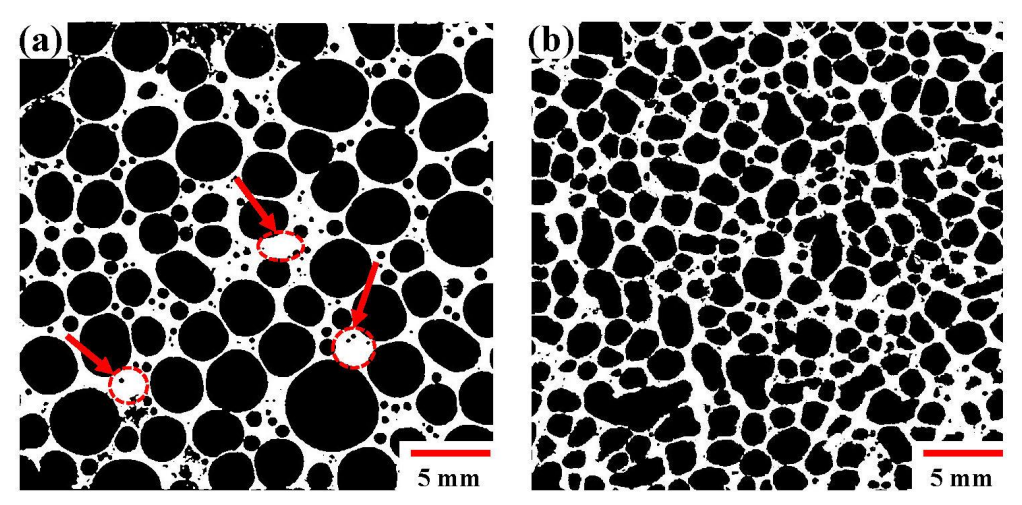


Fig. 7. Cross-sectional morphology of cells after binarization treatment: (a) AISiMg foam, (b) AICa foam.

The sequential deformation evolutions of AlSiMg and AlCa foams are Fig. 8 and 9, respectively, where red arrows indicate the loading direction. The strain distribution of the foam obtained by DIC method are calculated as shown in Figs. a1-a4, and the corresponding actual deformation is shown in Figs. b1 - b4. For AlSiMg foam, during the initial compression stage at ε = 0.07, deformation was concentrated around the large pores, as indicated by the red areas in Fig. 7 b2. This concentration resulted from the synergistic effect between large pores and hard phases. Large pores correspond to thinner cell walls per unit volume, making them more susceptible to deformation. Meanwhile, the presence of hard Si/Mg₂Si phases in the matrix leads to brittle fracture of the cell walls, hindering stress transmission and causing stress concentration. As compression proceeds, shear bands extend along the interfaces between the hard phases and MgAl₂O₄ particles, inducing localized deformation. As shown in Figs 8 a3 and 8 a4, the hard phases (Si/Mg₂Si) impede deformation, causing a sudden transition in the deformation distribution from blue to red. Additionally, localized spalling (Fig. 8 b3) and the formation of larger cracks (Fig. 8 b4) are observed. The dominant failure mode of AlSiMg foam is brittle shear fracture.

The overall deformation of AlCa foam is

relatively uniform, as depicted in Fig. 9 b2, with the strain distribution being more consistent and exhibiting no abrupt changes in the strain field, as observed in Fig. 9 a2. As compression progresses, an "X"-shaped deformation pattern emerges, as illustrated in Figs. 9 a3 and b3. The AlCa foam experiences overall plastic deformation without any apparent cracks or interface spalling, and the strain field remains uniformly distributed. The cell walls first buck and finally fracture.

Based on the above analysis, two deformation mechanism models for the foams are proposed: (1) "Hard-phase The support—Brittle deformation for AlSiMg foam. The hard phases (Si/Mg₂Si) form a high-stiffness framework that enhances the initial plateau stress, and the stress around concentration large pores initiates microcracks, as indicated by the DIC results. These cracks propagate along the interface between the hard phases and MgAl₂O₄, leading to local collapse and causing fluctuations in the stress-strain curve. (2) The AlCa foam failures in a "Plastic coordination—Progressive buckling" mode. Small-sized and uniformly distributed pores, coupled with a high-plasticity matrix, promote the coordinated bending of the cell walls. No interface spalling occurs, and energy is continuously absorbed through plastic dissipation in this deformation mode.



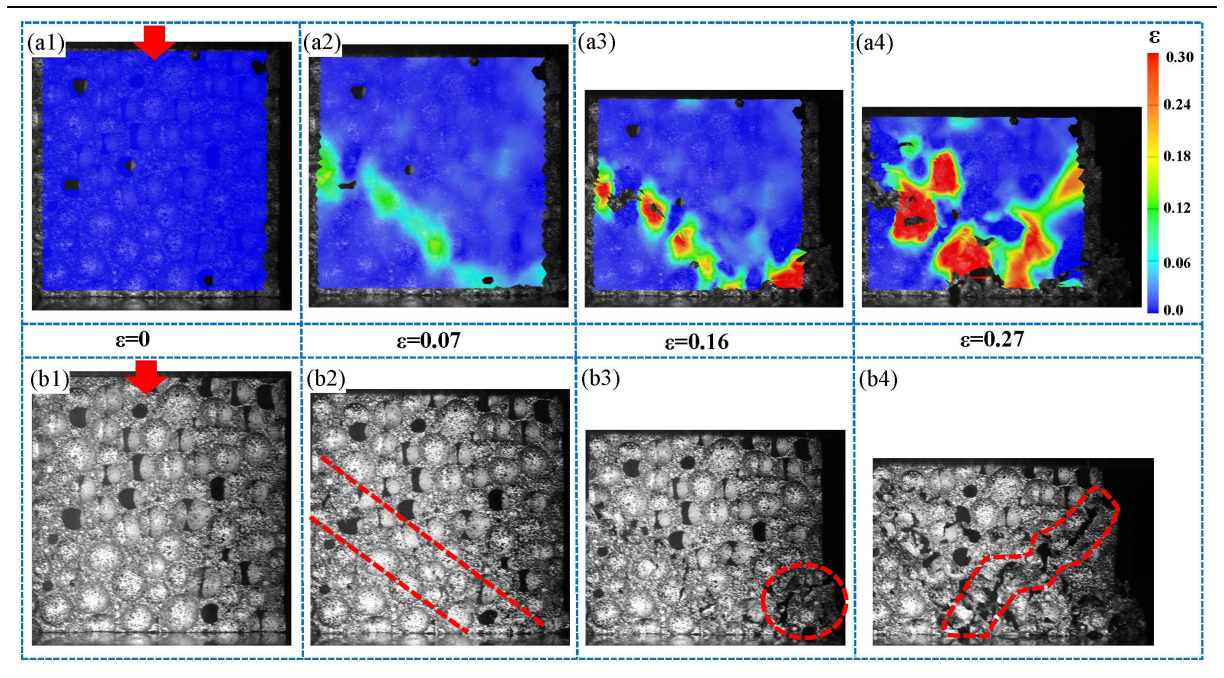


Fig. 8: Deformation evolutions of the AlSiMg foam, (a1) - (a4): Strain distribution within the foam obtained by DIC; (b1) - (b4):

Corresponding actual deformation.

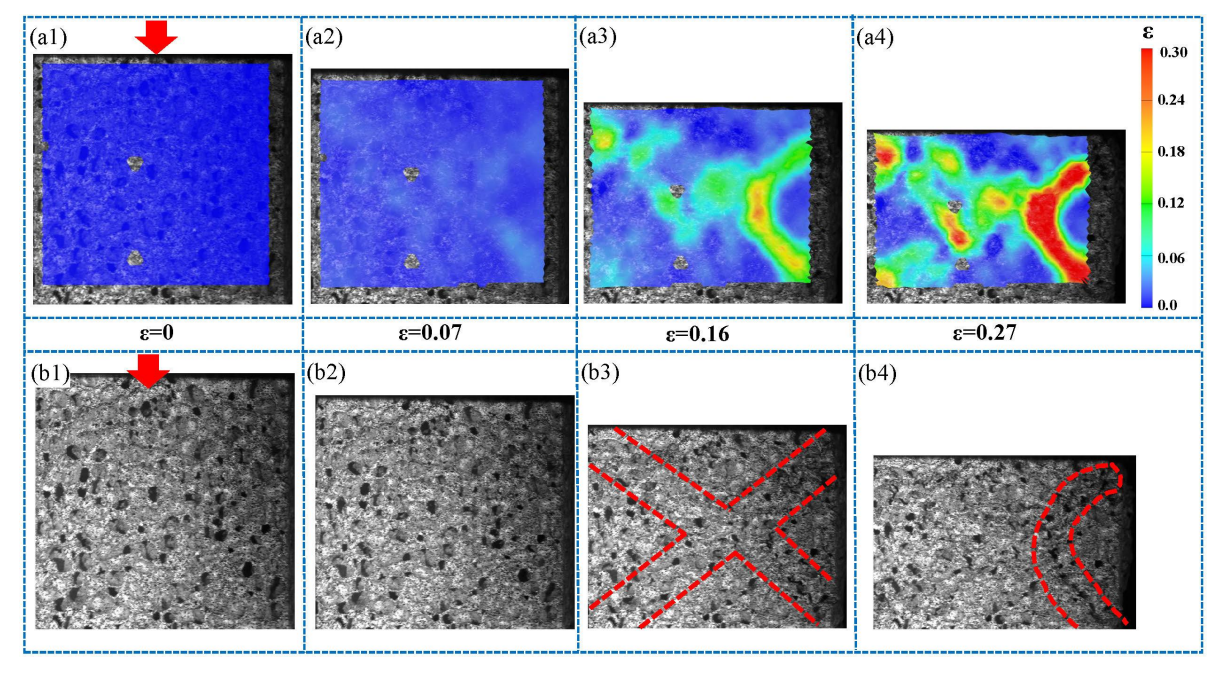


Fig. 9: Deformation evolutions of the AlCa foam, (a1) - (a4): Strain distribution within the foam obtained by DIC; (b1) - (b4):

Corresponding actual deformation.

4 Conclusions

By comparing and analyzing AlSiMg-based and traditional AlCa-based aluminum foams, the following conclusions have been drawn:

(1) For the Al-Ca foam, the stress varies between 8.6 and 14.8 MPa, with the plateau region length decreasing as relative density increases. In contrast,

the AlSiMg foam exhibits a significantly higher initial peak stress of 28.7 MPa at $\rho_r=0.25,$ nearly double that of the Al-Ca foam (14.8 MPa, $\rho_r=0.29)$ observed in the AlCa foam. Additionally, the stress-strain curve of the AlSiMg foam displays pronounced fluctuations in the plateau region compared to the AlCa foam.

- (2) The strength and superior ductility of AlCa foam are mainly attributed to the presence of the eutectic Al₄Ca phase. AlSiMg foam exhibits higher yield and plateau stresses due to the presence of hard secondary phases such as Mg₂Si and Si. However, these hard phases, together with micron-sized MgAl₂O₄ spinel particles, can induce brittle fracture during compression, leading to stress fluctuations in the stress–strain curves.
- (3) At low relative densities, the energy absorption performance of AlCa foam is superior to that of AlSiMg foam. Conversely, at higher relative densities, AlSiMg foam demonstrates superior energy absorption performance. Specifically, at a relative density of ρ_r =0.26, the maximum energy absorption efficiency of AlSiMg foam is approximately twice that of AlCa foam. The deformation mechanism of AlCa foam is characterized "Plastic by coordination—Progressive buckling " mode, while that of AlSiMg foam is defined by a "Hard-phase support—Brittle fracture" mode, in which cracks propagate along the hard-phase interfaces.

Acknowledgments

The authors would like to acknowledge the funding support by the Beijing Natural Science Foundation of China (Grant No. 3244034).

Conflicts of interest:

The authors declare that they have no known competing financial interests or personal relationships that could have appeared to influence the work reported in this paper.

References

- Banhart J. Manufacture, characterisation and application of cellular metals and metal foams.
 Progress in Materials Science, 2001, 46(6): 559-632.
- [2] Lefebvre L P, Banhart J, Dunand D. Porous Metals and Metallic Foams: Current Status and Recent Developments. Advanced Engineering Materials, 2010, 10(9): 775-787.

- [3] Cambronero L E G, Ca nadas I, Ruiz-Román, et al. Weld structure of joined aluminium foams with concentrated solar energy. Journal of Materials Processing Technology, 2014, 214(11): 2637-2643.
- [4] Guo-Yin Z U, Ri-Huan L U, Xiao-Bing L I, et al. Three-point bending behavior of aluminum foam sandwich with steel panel. Transactions of Nonferrous Metals Society of China, 2013, 23(9): 2491-2495.
- [5] Fu W, Li Y. Fabrication, processing, properties, and applications of closed-cell aluminum foams: a review. Materials, 2024, 17(3): 560.
- [6] Yuan G, Li Y, Zhou X, et al. Preparation of Complex Shaped Aluminum Foam by a Novel Casting-Foaming Method. Materials Letters, 2021, 293:129673.
- [7] Yuan G, Li Y, Hu L, et al. Preparation of shaped aluminum foam parts by investment casting. Journal of Materials Processing Technology, 2023, 314: 117897.
- [8] Fu W, Li Y. Air blowing assisted fabrication of Al–Si–Mg foams by melt-foaming route. Metallurgical and Materials Transactions B, 2025, [Published online]. DOI: 10.1007/s11663-025-03612-w.
- [9] Wang T, Zuo X, Zhou Y, et al. Stability mechanism of AlSi12 aluminum foam under the action of Al-Si-Ca second phase. Journal of Materials Research and Technology, 2021, 11: 1991-2002.
- [10] Gölbaşı Z, Oztürk B, Üllen N B. The structural and mechanical properties of open-cell aluminum foams: Dependency on porosity, pore size, and ceramic particle addition. Journal of Alloys and Compounds, 2024, 1009: 176921.
- [11] Sun K, Wang L, Wei G. et al. Recent advances and future trends in enhancing the compressive strength of aluminum matrix foam composites reinforced with ceramic hollow spheres: A review. Composite structures, 2024, 331: 117918.
- [12] Hu L, Li Y, Zhou X, et al. Characterization of as-cast microstructure of aluminum foams by melt foaming method. Materials Letters, 2022, 308: 131112.
- [13] Liu K, Chen C, Guo W, et al. Energy absorption



- and deformation behavior of multilayer aluminum foam structures. Materials Science & Engineering, A. Structural Materials: Properties, Misrostructure and Processing, 2022, 832: 142470.
- [14] Gibson L J, Ashby M F. Cellular solids: structure and properties. Cambridge University Press, 1997.
- [15] Cheng H F, Hang X M, XU L. Effect of Matrix Properties on Compressive Behavior and Energy Absorption of Foamed Al Alloys. Nonferrous Metals,2003, 55(3): 4.
- [16] Cheng H F, Hu K G, Xue G X, et al. Study of microstructure and compressive mechanical properties of aluminium foam alloys. Transactions of materials and heat treatment, 2005, 26(4): 5.
- [17] Huang L, Wang H, Yang D et al. Effects of scandium additions on mechanical properties of cellular Al-based foams. Intermetallics, 2012, 28: 71-76.
- [18] Xia X, Feng H, Zhang X, et al. The compressive properties of closed-cell aluminum foams with different Mn addition. Materials & Design, 2013, 51: 797-802.
- [19] Zhao W M, Zhang Z, Wang Y N, et al. Compressive characteristics of closed-cell aluminum foams with different percentages of Er element. China Foundry, 2016, 13(1): 36-41.
- [20] Fusheng H, Zhengang Z. The mechanical behavior of foamed aluminum. Journal of Materials Science, 1999, 34(2): 291-299.
- [21] Lin Y, Zhang Q, Wu G. Interfacial microstructure and compressive properties of Al-Mg syntactic foam reinforced with glass cenospheres. Journal of Alloys and Compounds, 2015, 655: 301-308.
- [22] Lohani D, Daniel B S S. Influence of Al₂O₃ additives on mechanical properties and energy absorption in closed-cell aluminum foam fabricated

- via friction stir processing. Transactions of the Indian Institute of Metals, 2025, 78(4): 83.
- [23] Miyoshi T. Aluminum foam" ALPORAS": The production process, properties and applications. Metal Foams and Porous Metal Structures, 1999, 521: 133.
- [24] Körner C, Singer R F. Processing of metal foams—challenges and opportunities. Advanced Engineering Materials, 2000, 2(4): 159-165.
- [25] Zhou X, Li Y, Chen X. Development of AlMg35-TiH2 composite foaming agent and fabrication of small pore size aluminium foams. Journal of Materials Processing Technology, 2020, 283: 116698.
- [26] Wang N Z, Chen X, Li Y X, et al. Preparation and compressive performance of an A356 matrix syntactic foam. Materials Transactions, 2018, 59(5): 699-705.
- [27] Andrews E, Sanders W, Gibson L J. Compressive and tensile behaviour of aluminum foams. Materials Science & Engineering A, 1999, 270(2): 113-124.
- [28] Wang T, Zuo X, Yi J, et al. Enhancing melt foam stability, form-filling process, and pore structure evolution of shaped aluminum foam. Journal of Materials Research and Technology, 2024, 33: 5708-5719.
- [29] Cox H L. The elasticity and strength of paper and other fibrous materials. British J of Applied Physics, 1951, 3(3): 72.
- [30] Jin Y, Fang H, Chen R, et al. Morphological modification of Mg₂Si phase and strengthening mechanism in Mg₂Si/Al composites by Eu addition and T6 heat treatment. Journal of Materials Science & Technology, 2023, 159: 151-162.